npj | climate and atmospheric science

Article

Published in partnership with CECCR at King Abdulaziz University

https://doi.org/10.1038/s41612-026-01384-x

Enhanced persistence of Ural blocking under strong positive AO: the role of North Atlantic storm tracks and potential vorticity dynamics

Ho-Young Ku[1], Hayeon Noh[2], Muyin Wang[3,4], James Overland[4], Seong-Joong Kim[5,6] & Baek-Min Kim[1]

Ural blocking (UB) and the associated Warm Arctic–Cold Eurasia (WACE) pattern are typically linked to the negative Arctic Oscillation (AO). However, robust UB events are surprisingly observed even during the positive AO phase, a condition generally expected to suppress blocking due to enhanced zonal flow. This study investigates how positive AO magnitude modulates UB persistence. We find that under strong positive AO conditions (AO > +1), UB events persist significantly longer (6.1 days) than weak positive AO (4.7 days). This enhanced persistence results from organized North Atlantic storm tracks that facilitate intense heat and moisture into the Barents–Kara Sea. The resulting Arctic warming and sea ice loss trigger a thermodynamic feedback loop that weakens the meridional potential vorticity (PV) gradient, effectively anchoring the UB system. Our findings reveal that strong positive AO paradoxically promotes persistent blocking through storm-PV coupling, offering critical insights for improving sub-seasonal predictions of Eurasian winter extremes.

The Arctic Oscillation (AO) is the dominant mode of Northern Hemisphere atmospheric variability, exerting a profound influence on wintertime circulation patterns and climate extremes[1,2]. By modulating the strength and latitudinal position of the midlatitude westerlies, the AO governs large-scale wave activity, storm tracks, and sea ice distribution in the Arctic[3,4].

Traditionally, the relationship between the AO (or its Atlantic manifestation, the North Atlantic Oscillation; NAO) and atmospheric blocking—specifically Ural blocking (UB)—has been interpreted through the lens of mean flow strength[4–7]. The negative phase of these modes, characterized by weakened midlatitude westerlies and enhanced meridional flow, is widely regarded as the favorable background condition for frequent blocking formation and the associated Warm Arctic–Cold Eurasia (WACE) pattern[8–10]. Conversely, the positive phase is generally considered to suppress blocking due to enhanced zonal confinement of the jet stream[11,12].

In this study, we utilize the AO index as the primary atmospheric mode to investigate its relationship with UB persistence, building on the dynamical framework established by prior studies. Notably, Luo et al.[5] demonstrated that the positive phase of the NAO can promote UB formation through Rossby wave dynamics. While the AO and NAO share significant variance over the North Atlantic, the AO exhibits a more distinct northeastward extension of the upper-tropospheric jet toward the Barents-Kara Sea (BKS) compared to the NAO (Figure S1). This structural feature makes the AO particularly suitable for explaining the poleward intrusion of synoptic storms into the Arctic[13]. In this context, we prioritize the AO as a key modulator to explore the impacts of the positive phase on UB.

Recent studies have highlighted that the onset of UB and rapid Arctic warming is frequently driven by the intrusion of intense cyclones into the Arctic[14,15]. These storms facilitate intense poleward heat and moisture transport, which accelerates sea ice loss and amplifies downward longwave radiation, creating a feedback loop that reinforces blocking persistence[16,17]. Crucially, the dynamic pathway for these storms to penetrate deep into the Arctic is paradoxically favored under the positive AO phase. Stronger westerlies associated with a positive AO can extend the North Atlantic storm track poleward, directing energy and moisture toward the BKS region[18–20].

A prime example is the January 2016 event, where Storm Frank—a powerful cyclone occurring under strong positive AO conditions—triggered extreme Arctic warming and a prolonged UB event[14]. This case suggests that the positive AO phase is not merely a blocking-suppressing regime but can

[1]Division of Earth Environmental System Sciences Major of Environmental Atmospheric Sciences, Pukyong National University, Busan, South Korea. [2]Climate and Environmental Research Institute, Korea Institute of Science and Technology, Seoul, Republic of Korea. [3]Cooperative Institute for Climate, Ocean, and Ecosystem Studies, University of Washington, Seattle, WA, USA. [4]NOAA/Pacific Marine Environmental Laboratory, Seattle, WA, USA. [5]Office of Vice President, Korea Polar Research Institute, Incheon, South Korea. [6]KOPRI School, University of Science and Technology, Incheon, South Korea. e-mail: baekmin@pknu.ac.kr

act as a potent driver of blocking when it is strong enough to facilitate deep storm intrusion and subsequent wave breaking. Consistent with this, this study has verified that a "strong" positive AO establishes a distinct storm-driven dynamical link to UB, a feature that is less evident under "weak" positive AO conditions.

Despite these insights, previous research has largely focused on inter-phase contrasts (positive vs. negative AO), leaving the intra-phase variability of the positive AO unexplored. Specifically, it remains unclear how variations in positive AO amplitude modulate the efficiency of storm track extension, Arctic heating, and the resultant UB duration. Neglecting this magnitude-dependent mechanism limits our understanding of why robust WACE patterns can emerge even when the background circulation (i.e., positive AO) theoretically opposes them.

Motivated by this gap, this study focuses on the positive AO phase, specifically distinguishing between strong and weak regimes, to elucidate the threshold-dependent mechanisms governing UB persistence. Crucially, we emphasize the AO-magnitude-dependent storm track shift as the key element that ties together the large-scale AO regime and the subsequent thermodynamic feedback loop. By examining how the magnitude of the positive AO index modulates the poleward steering of North Atlantic storms, we identify the specific dynamical pathway that facilitates the heat and moisture transport necessary for sustained blocking.

This paper is organized as follows. The results of our analysis on UB persistence, storm track dynamics, and potential vorticity evolution under strong versus weak positive AO conditions are first presented. Then, we provide a summary and discussion regarding the broader implications for Arctic–midlatitude linkages and the WACE pattern. Finally, the data and methodologies used in this study are described.

Results

Positive Arctic Oscillation magnitude modulates North Atlantic storm organization and penetration into the Arctic

The processes of storm-driven Arctic warming are closely linked to AO variability, as Arctic cyclone activity varies in tandem with AO phases[13]. To capture these interactions, we examine the trajectories of individual storm events based on the AO amplitude. Our tracking analysis of individual storm trajectories (Fig. 1) shows storm tracks more frequently extend into the Arctic—particularly over the BKS—as the AO magnitude increases. This facilitates poleward energy transport and surface warming that may precondition the region for UB formation.

Notably, even within the positive AO phase, storm penetration varies with AO magnitude at the time of the storm's maximum intensity (i.e., the date of minimum central SLP). When the AO index exceeds +1 standard deviation (σ), approximately 71.6% of storms reach the Arctic (Fig. 1a). In contrast, during moderate positive AO phases (0 < AO Index ≤ +1 σ), this fraction drops to about 55% (Fig. 1b). Consistent with these results, the binned analysis in Fig. 1e demonstrates a clear upward trend in the Arctic-entering ratio as the AO magnitude strengthens. Specifically, for AO values exceeding +1 σ, the ratio consistently remains above 60% and reaches as high as 100% in certain high-magnitude bins, further confirming the robust steering effect of a strong AO phase.

This behavior is consistent with the AO's characteristic pressure structure, which involves a tighter linkage to the Azores–Icelandic pressure dipole and a northeastward extension of the upper-tropospheric jet stream (Figure S1). When the AO magnitude exceeds +1 σ, this modified jet structure effectively steers synoptic-scale cyclones toward the BKS, rather than keeping them zonally confined in the mid-latitudes. These findings highlight the nonlinear influence of AO amplitude in organizing storm activity and regulating poleward heat transport into the Arctic.

Characteristics of Ural blocking under different AO conditions

To examine how AO magnitude influences UB characteristics, we classified UB events into two groups based on the Climate Prediction Center (CPC) AO index averaged from 7 to 3 days before UB onset (see "Methods" section): Strong Positive AO (SPAO) UB (18 events) and Weak Positive AO (WPAO) UB (15 events). Figure 2 compares the spatial distribution, duration, and intensity of UB events under these two conditions.

Figure 2a, d show the spatial distribution of UB events under SPAO and WPAO. In both conditions, UB events occur most frequently between 60°–70°N latitude band: 10 out of 18 events (56%) for SPAO and 7 out of 15 events (47%) for WPAO (Fig. 2a, d).

In contrast, the mean duration of UB events is longer under SPAO (6.1 days) than under WPAO (4.7 days); the difference (1.4 days, ~30% increase) is marginally significant ($p \approx 0.1$, two-tailed t-test), indicating that stronger positive AO phases are associated with more persistent blocking events (Fig. 2b, d). This relationship is further supported by a scatter plot showing a marginal but physically consistent positive correlation ($r = 0.33, p = 0.055$) between the positive AO magnitude and the UB duration (Figure S2).

The intensity histograms (Fig. 2c, f) show that UB events under SPAO tend to be stronger, with a peak frequency in the 300–400 gpm range, while those under WPAO peak in the 200–300 gpm range. On average, blocking intensity is slightly higher under SPAO (340 gpm) than under WPAO (326 gpm), although this difference is not statistically significant.

Large-scale circulation patterns and wave propagation

To compare the large-scale atmospheric patterns associated with UB under different AO conditions, we analyzed composite maps of detrended 2-m temperature (T2M) anomalies, 500-hPa GPH anomalies, and wave activity flux (WAF) from Lag −3 to +8 days relative to blocking onset (Fig. 3). The key differences between the two AO conditions are examined below.

At Lag -3 days, SPAO shows no pre-existing WACE pattern, with relatively neutral temperature conditions across both Arctic and Eurasian regions. A distinct dipole structure between the Icelandic Low and the Azores High is evident under SPAO, leading to pronounced wave propagation over the North Atlantic (Fig. 3a). In contrast, WPAO already exhibits a well-established pattern resembling WACE before blocking onset, with the low-pressure system shifted eastward toward Europe, resulting in a more zonal wave propagation pattern (Fig. 3b). Crucially, high-pressure anomalies and positive T2M anomalies are already present over northern Siberia, while negative T2M anomalies extend across the southern and central parts of the Eurasian continent.

At UB onset, under SPAO wave propagation from the North Atlantic is enhanced, reinforcing a high-pressure anomaly over the Ural region, centered over the BKS (Fig. 3c). This is accompanied by significant positive T2M anomalies in the Arctic region. In contrast, under WPAO, wave propagation from Europe to the Ural region is more dominant, and the high-pressure anomaly is centered slightly farther south (Fig. 3d).

At Lag +4 days, under SPAO, Arctic warming intensifies, with T2M anomalies exceeding 8 °C over the BKS. The well-developed high-pressure system over the Ural region facilitates strong downstream wave propagation into CEU, forming a pronounced cold anomaly (Fig. 3e). Under WPAO, wave propagation from the Ural high-pressure system into Eurasia is also evident, but the cold anomaly is weaker, more diffuse, and extends farther eastward into East Asia at a faster rate (Fig. 3f).

At Lag +8 days, the high-pressure anomaly over the Ural region persists under SPAO, reinforcing the cold anomaly over CEU and extending into East Asia (Fig. 3g). Meanwhile, Arctic warming over the BKS remains strong. Under WPAO, however, Arctic warming weakens significantly. The high-pressure system shifts westward, intensifying the cold anomaly over Europe and western Eurasia (Fig. 3h).

Overall, the evolution of the WACE pattern differs fundamentally between the two conditions. In SPAO, the WACE pattern undergoes dynamic development where intense wave propagation from the North Atlantic actively creates the anomalies from initially neutral conditions. This results in a concentrated and robust cooling center over Central Eurasia, directly downstream of the anchored UB.

In contrast, WPAO reflects a migratory evolution of pre-existing WACE-like conditions. Under WPAO, the relatively weakened midlatitude westerlies compared to SPAO reduce the eastward phase speed of the

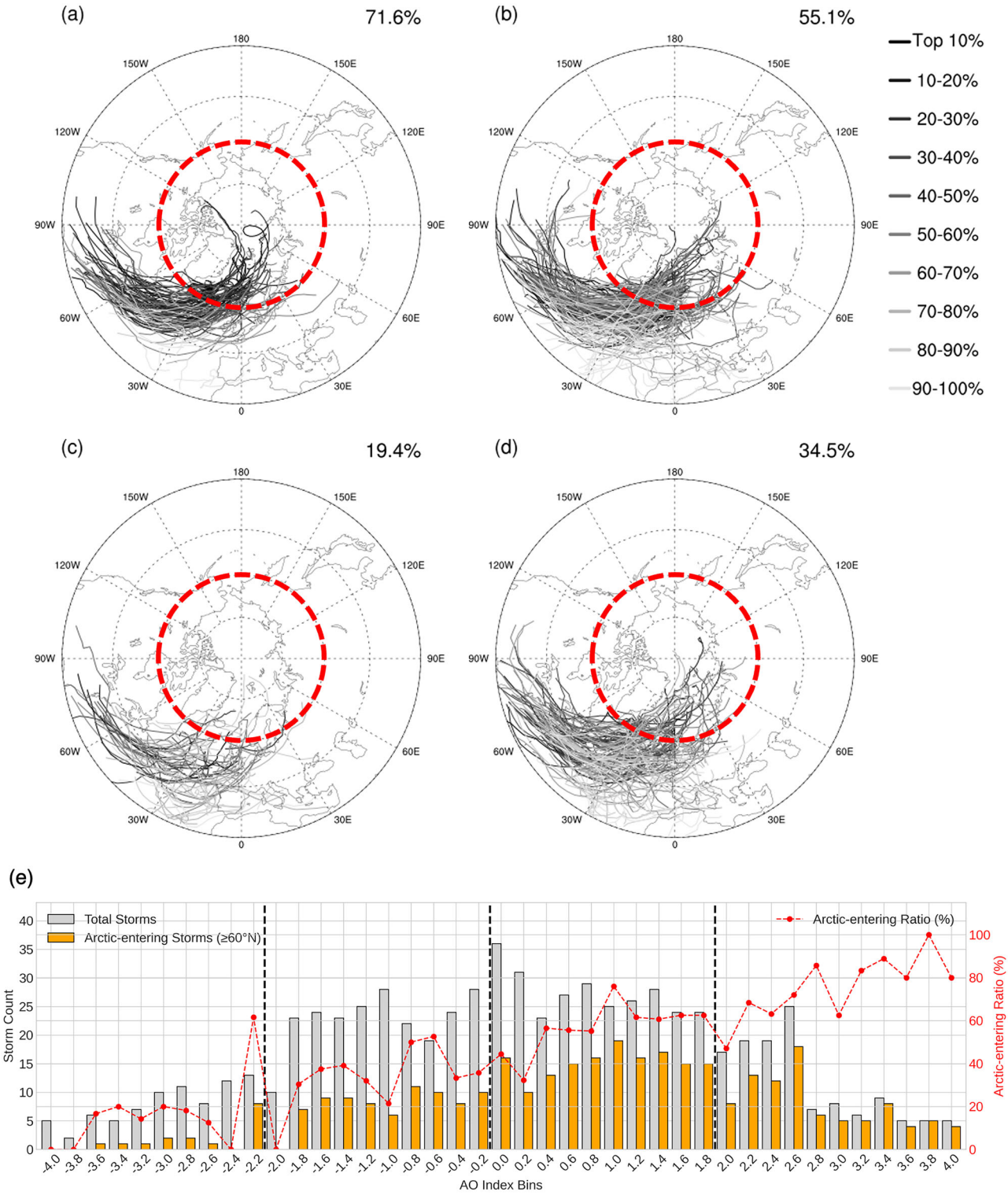

Fig. 1 | North Atlantic winter storm tracks and Arctic entry rates stratified by the Arctic Oscillation (AO) index. Individual storm trajectories are shown for four AO regimes defined by the AO magnitude at each storm's peak intensity date: **a** AO Index >+1 σ, **b** 0 < AO Index ≤ +1 σ, **c** AO Index <−1 σ, and **d** −1 σ ≤ AO Index < 0. Here, 1 σ corresponds to the wintertime (DJF) standard deviation of the daily AO index (approximately 1.95). Each line represents an individual storm track, with shades of gray indicating storm intensity percentiles based on central pressure, where darker lines denote stronger cyclones (as indicated in the legend). The red dashed circle marks the Arctic domain (≥60°N). The percentage in the top-right of each panel indicates the fraction of storms that entered the Arctic under each AO regime. **e** Storm frequency binned by AO index magnitude (0.2 intervals), where gray bars represent the total number of storms and yellow bars indicate the number of Arctic-entering storms (≥60°N). The red dashed line shows the corresponding Arctic-entering ratio (%). Vertical dashed lines in (**e**) mark the +1 σ and −1 σ thresholds.

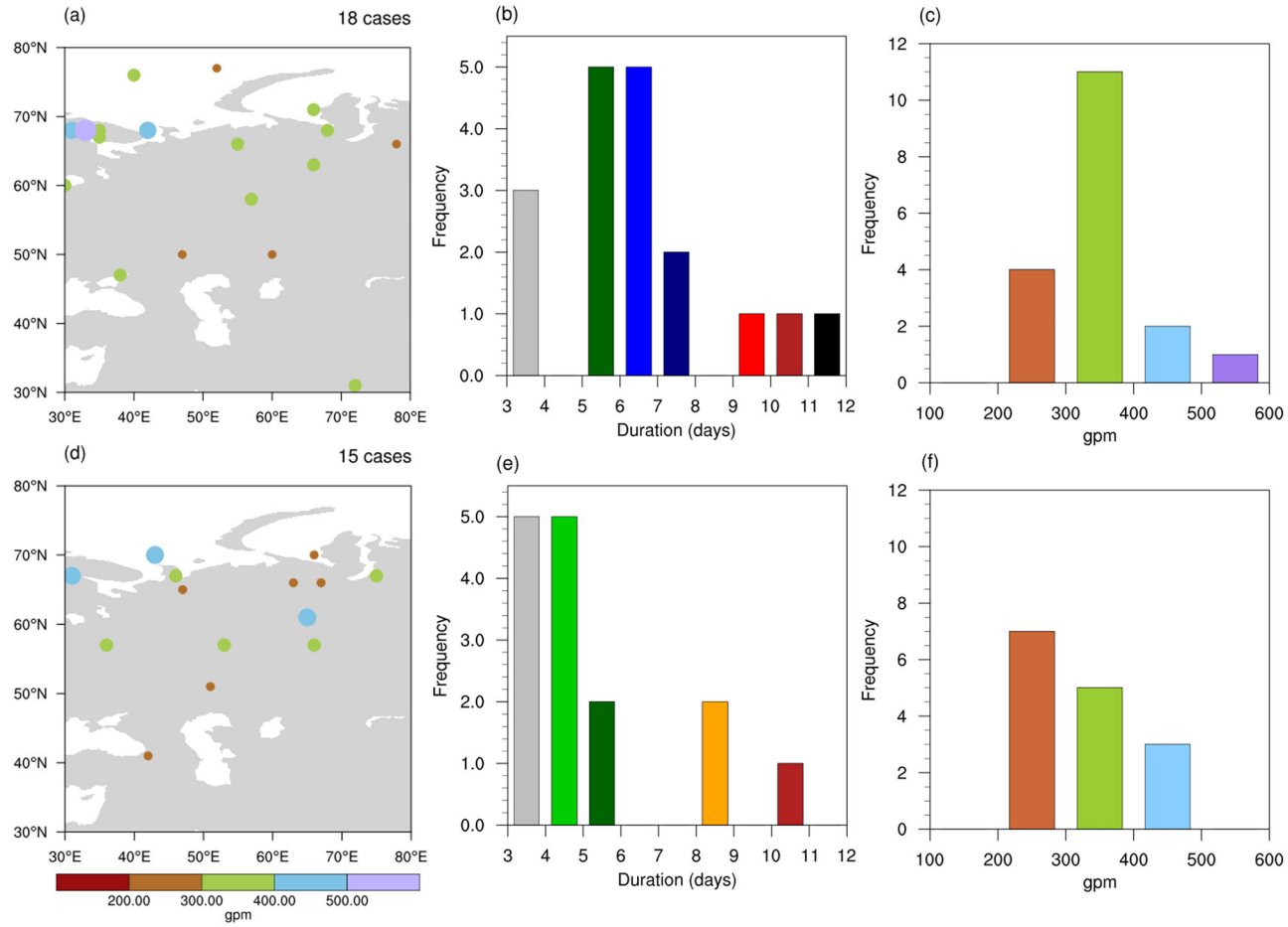

Fig. 2 | Ural Blocking (UB) event characteristics under positive Arctic Oscillation (AO) regimes. a–c UB events identified during strong positive AO (SPAO; 18 events): **a** spatial distribution of blocking events, **b** histogram of blocking duration (days), and **c** histogram of blocking intensity measured as 500-hPa geopotential height (GPH) anomaly (gpm). **d–f** Same as (**a–c**), but for weak positive AO (WPAO; 15 events).

system, providing a favorable environment for the UB to shift westward. This migration is accompanied by suppressed synoptic eddy activities, which trigger a nonlinear eddy-to-mean flow feedback[21] that induces a broad Arctic-warming and Eurasian-cooling dipole. Consequently, the WPAO regime produces a more diffuse WACE pattern that migrates from Central Eurasia toward Western Europe.

Influence of North Atlantic storms on Ural blocking and surface response

To investigate the role of North Atlantic storm activity and upper-level jet structure in UB development under different AO conditions, we analyzed storm tracks during the seven days preceding UB onset and 300-hPa zonal wind averaged over Lag −7 to −3 days (Fig. 4).

Although the storm count per UB event is slightly higher under SPAO (1.6) than WPAO (1.3), this difference is not statistically significant. In contrast, the spatial patterns of storm tracks show more pronounced differences. Under SPAO conditions (Fig. 4a), storms follow a coherent path along the Gulf Stream with limited meridional spread, regardless of intensity. In WPAO (Fig. 4b), on the other hand, tracks are more scattered and irregular, reflecting weaker steering by the large-scale flow.

The spatial differences in storm tracks are closely linked to the upper-level jet structure. Under SPAO (Fig. 4c), the 300-hPa jet core is located farther south and extends poleward, enhancing poleward warm air transport and contributing to BKS warming. In contrast, under WPAO (Fig. 4d), the jet shifts slightly northward and becomes more zonal over Europe, favoring more zonal wave propagation and weaker warm advection into the Arctic.

Climatological composites of 300-hPa zonal wind (Figure. S3) further show a stronger and more extensive westerly jet under SPAO, with wind speeds exceeding +8 m/s from the North Atlantic to the Ural region (~60°W–60°E). This stronger jet enhances wave propagation and guides North Atlantic storms along a more poleward trajectory[22,23], effectively acting as a focused waveguide that minimizes meridional scattering. This highly organized transport facilitates increased warm air transport into the Arctic and reinforces BKS warming.

These results highlight the key role of storm tracks and jet structure in modulating Arctic warming and UB formation. Under SPAO, storms follow organized, poleward paths that enhance BKS warming and support prolonged UB (Fig. 3c, e, g). In contrast, weaker jet guidance under weak AO leads to scattered storm paths, weaker warming, and shorter-lived blocking (Fig. 3d, f, h).

This difference in storm organization leads to a distinct separation in poleward energy transport efficiency. To quantify this, we examine the composite of Meridional Eddy Heat Flux (v'T') and Meridional Eddy Moisture Flux (v'Q') at 850 hPa on the UB onset date (Fig. 5). Under SPAO conditions (Fig. 5a, c), there is a pronounced, statistically significant northward transport of heat and moisture extending from the North Atlantic into the BKS region. This intense flux is consistent with the organized, poleward-shifted storm tracks shown in Fig. 4a. Specifically, the strong positive v'T' anomaly over the BKS region demonstrates that the coherently organized storms under SPAO are highly effective at

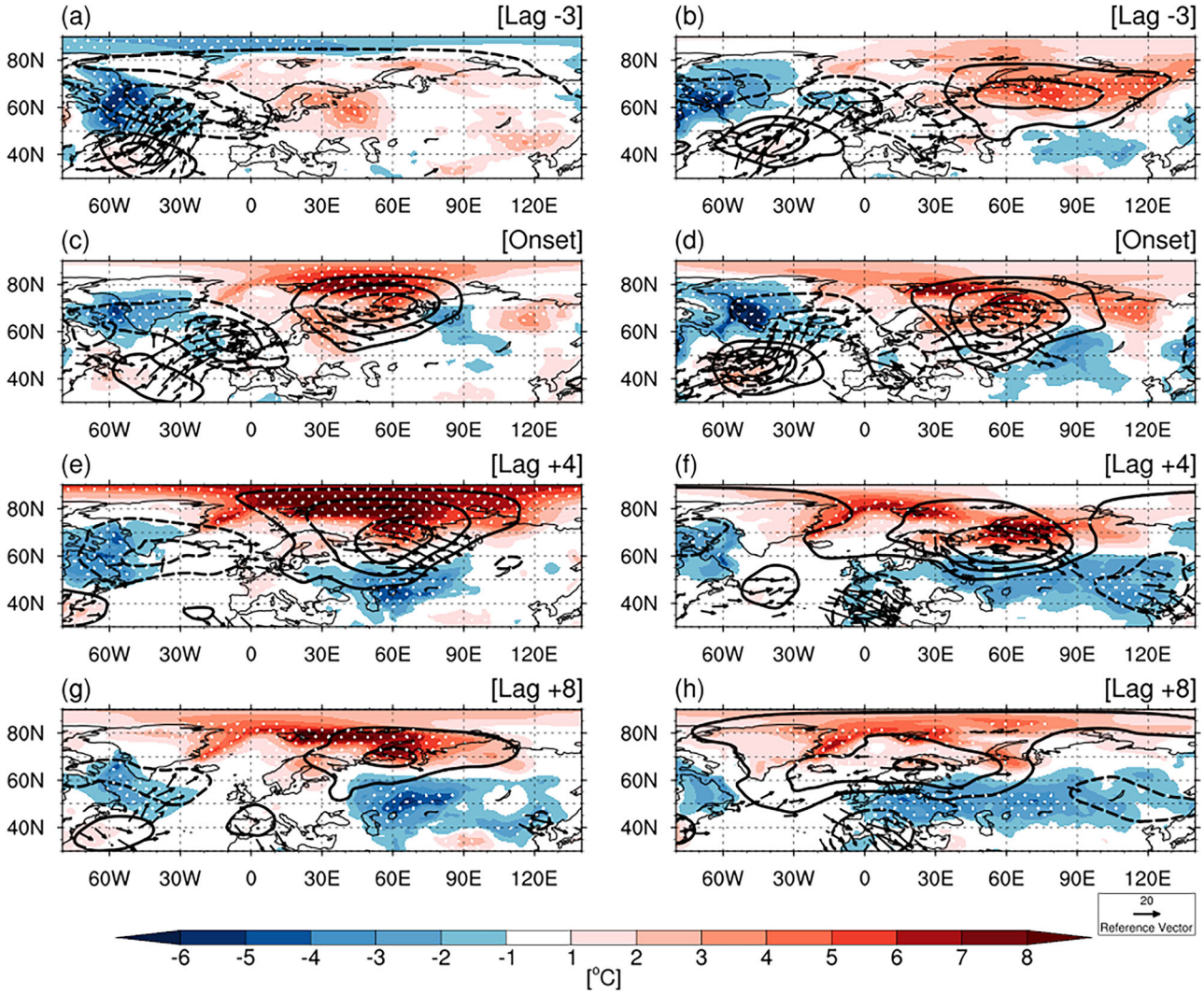

Fig. 3 | Composite anomaly maps for Ural Blocking events under strong and weak positive AO regimes at selected lag times. Each panel shows detrended 2-m temperature anomalies (shading, °C), 500-hPa geopotential height anomalies (contours, gpm), and wave activity flux (vectors, $m^2 \cdot s^{-2}$) for UB events under (left) SPAO and (right) WPAO at: **a**, **b** Lag −3 days, **c**, **d** onset date, **e**, **f** Lag +4 days, and **g**, **h** Lag +8 days. White dots indicate temperature anomalies statistically significant at the 95% confidence level based on a two-tailed Student's *t* test.

transporting warm air masses into the high Arctic. Similarly, the enhanced v'Q' flux suggests significant moisture advection, which is critical for strengthening DLR feedback.

In contrast, under WPAO conditions (Fig. 5b, d), the positive anomalies of both heat and moisture fluxes are significantly weaker, more diffuse, and lack the coherent high-latitude extension observed in SPAO events. This reflects the scattered storm tracks and weaker jet guidance under WPAO, resulting in less efficient energy transport into the Arctic. A difference map further indicates that the moisture transport (v'Q') under SPAO is more intense than under WPAO, particularly over the BKS entrance (Figure S4b). These results suggest that the magnitude of the positive AO phase acts as a critical modulator of poleward energy transport, directly determining the thermodynamic precondition for prolonged UB.

To further investigate how these differences in storm tracks and jet structure influence regional thermodynamic feedback, we analyzed atmospheric and surface variables from Lag −7 to +14 days relative to UB onset (Fig. 6). The time series illustrates the evolution of T2M, SIC, DLR, LHF, and SHF over the BKS, as well as T2M changes in CEU.

Over the BKS, T2M rises sharply under SPAO, initiating ~2 days before UB onset and peaking at +8 °C by Lag +4 days (Fig. 6a). This warming precedes UB intensification and aligns with enhanced warm advection from more frequent, poleward-shifted Atlantic storms (Fig. 4a), reinforcing feedback. In contrast, WPAO is associated with a slower T2M increase, peaking at +6 °C after UB onset, reflecting reduced storm influence.

Under SPAO, BKS warming coincides with a marked increase in DLR (~ 40 W/m² from Lag -2 to +3 days; Fig. 6b). This radiative enhancement is physically supported by the intensified poleward moisture transport (v'Q') observed in Fig. 5, which facilitates the accumulation of atmospheric moisture and cloud cover over the BKS. In contrast, under WPAO, DLR increases more modestly (~20 W/m²), suggesting a less efficient radiative feedback and weaker Arctic warming.

Surface fluxes further distinguish the two regimes (Fig. 6c, d). Under SPAO, SHF and LHF decline before UB onset—by ~15 and ~5 W/m², respectively—suggesting reduced oceanic heat loss due to diminished air–sea temperature gradients and suppressed surface evaporation. In contrast, under WPAO, LHF and SHF fluctuate within ±10 W/m² without a clear trend, indicating weaker air–sea coupling and less coherent warm air transport. By Lag +13 to +14 days, both fluxes rise under SPAO, reflecting secondary air–sea interactions triggered by sea ice loss and enhanced heat–moisture exchange.

SIC shows a sustained and statistically significant decline under SPAO from Lag −3 to +14 days (Fig. 6e), consistent with enhanced warming and reduced heat flux. In contrast, no notable SIC reduction occurs under weak AO, indicating insufficient warming. This is consistent with Luo et al.[18], who

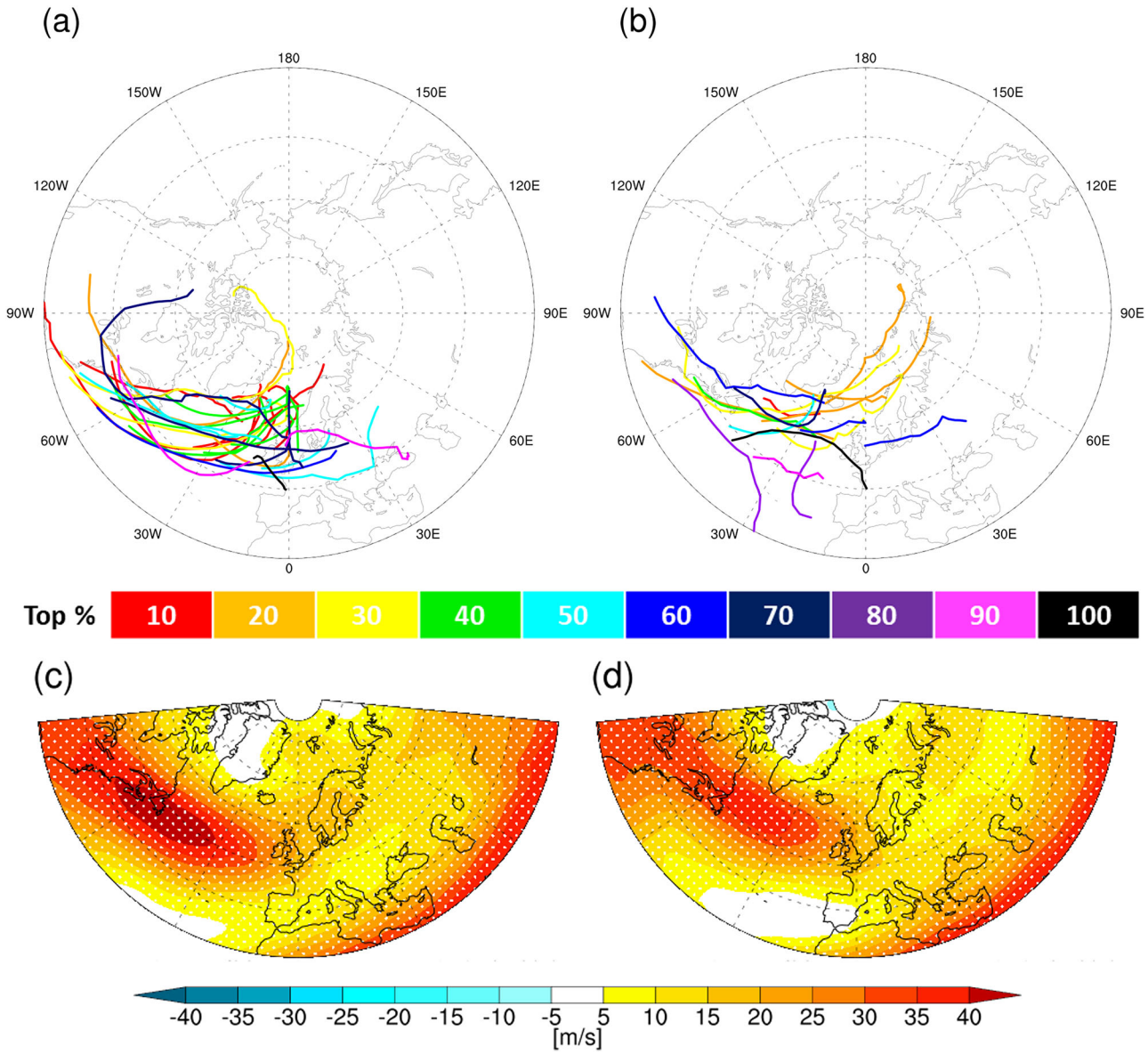

Fig. 4 | North Atlantic storm tracks and upper-level zonal wind anomalies during the pre-onset period of Ural Blocking events under SPAO and WPAO. a, **b** Storm tracks during the 7 days preceding UB onset under **a** SPAO (18 events) and **b** WPAO (15 events); line colors represent storm intensity percentiles, where red (top 0–10%) indicates the strongest storms and black (90–100%) the weakest. **c**, **d** Composite maps of 300-hPa zonal wind anomalies (shading, m/s) averaged over Lag −7 to −3 days before UB onset for **c** SPAO and **d** WPAO. White dots indicate regions of statistical significance at the 95% confidence level based on a two-tailed Student's *t* test.

showed that UB events co-occurring with a positive NAO phase induce the strongest SIC decline via increased poleward heat and moisture transport. Similarly, our results indicate that under SPAO, UB is associated with the significant SIC loss[7], reinforcing the role of warm air advection and radiative feedback in Arctic warming.

Supplementary regression analysis (Figure S5) shows that higher AO indices are significantly associated with reduced SIC over the BKS, even in the absence of blocking. This indicates that a stronger positive AO can precondition the Arctic for more active air–sea interactions, enhancing surface warming via DLR-driven radiative feedback and subsequent SHF/LHF responses. These results align with modeling studies[17], which demonstrate that extensive sea ice coverage inhibits ocean–atmosphere coupling, thereby limiting Arctic warming and reducing UB persistence.

CEU, a downstream region where cold advection associated with UB plays a significant role in temperature variability[4,24,25], exhibits distinct responses under different AO conditions (Fig. 6f). Under SPAO, CEU initially experiences slight warming, followed by a sharp cooling beginning just before UB onset and reaching a minimum of −2.5 °C by Lag +7 days. This pattern reflects stronger cold air advection and the downstream influence of a persistent UB. Under WPAO, cold anomalies emerge earlier but intensify more gradually, stabilizing around −2.5 °C by Lag +11 days. These differences suggest that stronger AO conditions are associated with more abrupt and dynamic cold surges in CEU, reinforcing the eastward extension of the WACE pattern.

Overall, these results highlight distinct atmospheric and surface responses to UB under different positive AO conditions. Under SPAO, intensified North Atlantic storms lead to rapid Arctic warming, driven by enhanced DLR and radiative feedback, with suppressed SHF sustaining warming, sustained SIC reduction enhancing air–sea interactions, and secondary SHF/LHF increases by Lag +13 to +14 days. Supplementary regression analysis (Figure. S5) suggests that a higher AO index preconditions the Arctic for reduced SIC, enabling more effective DLR-driven

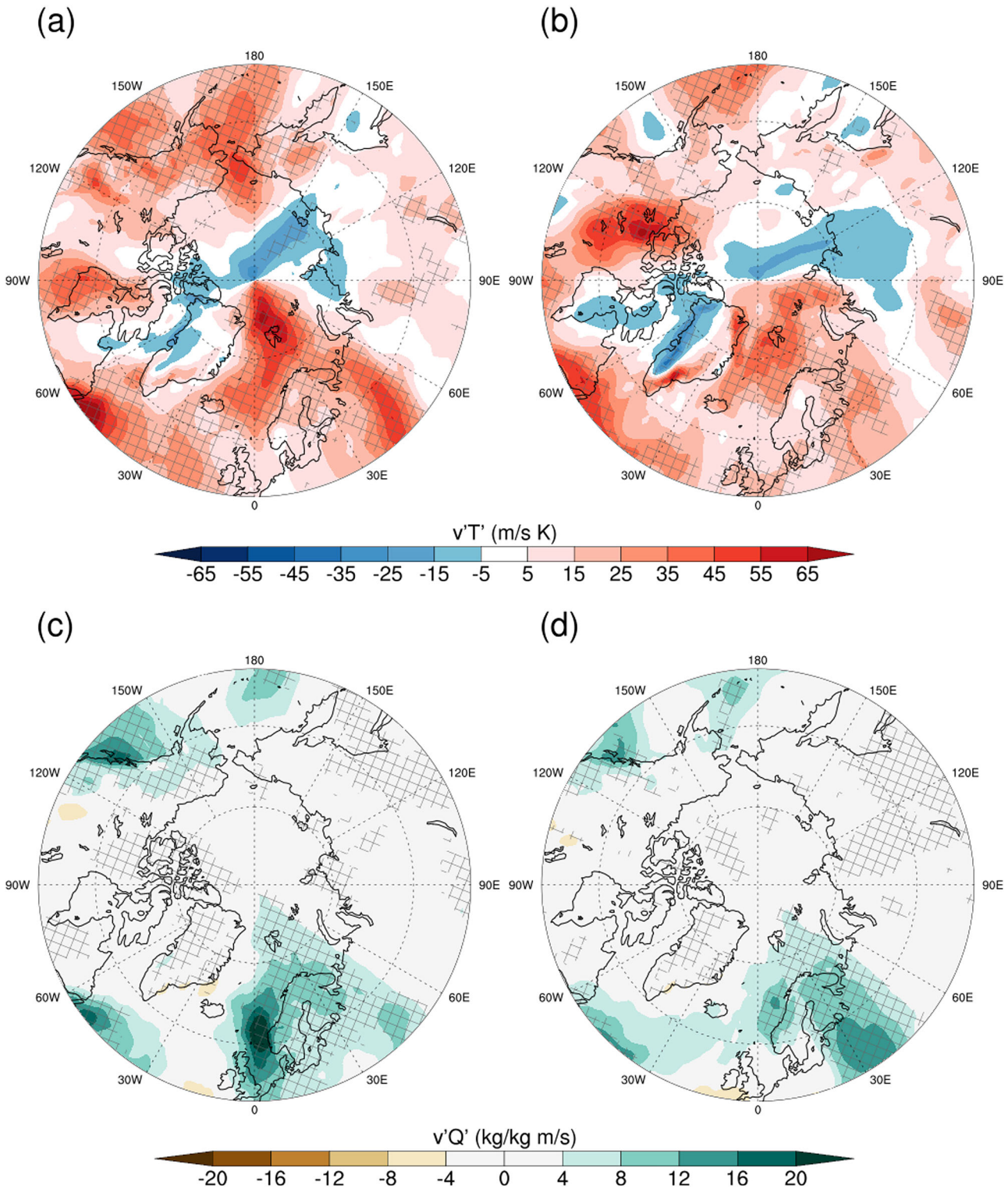

Fig. 5 | Composite maps of low-level eddy heat and moisture fluxes on the onset date of Ural Blocking events under SPAO and WPAO. a, **b** 850-hPa Meridional Eddy Heat Flux (v'T', K·m/s) and **c**, **d** 850-hPa Meridional Eddy Moisture Flux (v'Q', kg/kg·m/s) composited on the UB onset date for **a**, **c** SPAO (18 events) and **b**, **d** WPAO (15 events). Hatched areas indicate regions that are statistically significant at the 95% confidence level based on a two-tailed Student's *t* test.

feedback. Crucially, this comprehensive thermodynamic preconditioning is widely absent under WPAO, explaining the significantly shorter duration of UB events despite similar initial large-scale circulation anomalies.

These processes resemble the 2015/16 Arctic warming event described by Overland et al.[16], where a strong Atlantic storm under positive AO conditions triggered abrupt warming, sea ice loss, and prolonged UB. In contrast, under WPAO, these mechanisms are less active—resulting in more gradual warming, limited SIC decline, and minimal heat flux changes. CEU also experiences stronger and more variable cold anomalies under strong AO, further reinforcing the WACE pattern. These findings underscore the importance of storm activity, radiative feedback, and air–sea interactions in shaping UB characteristics and downstream climate impacts.

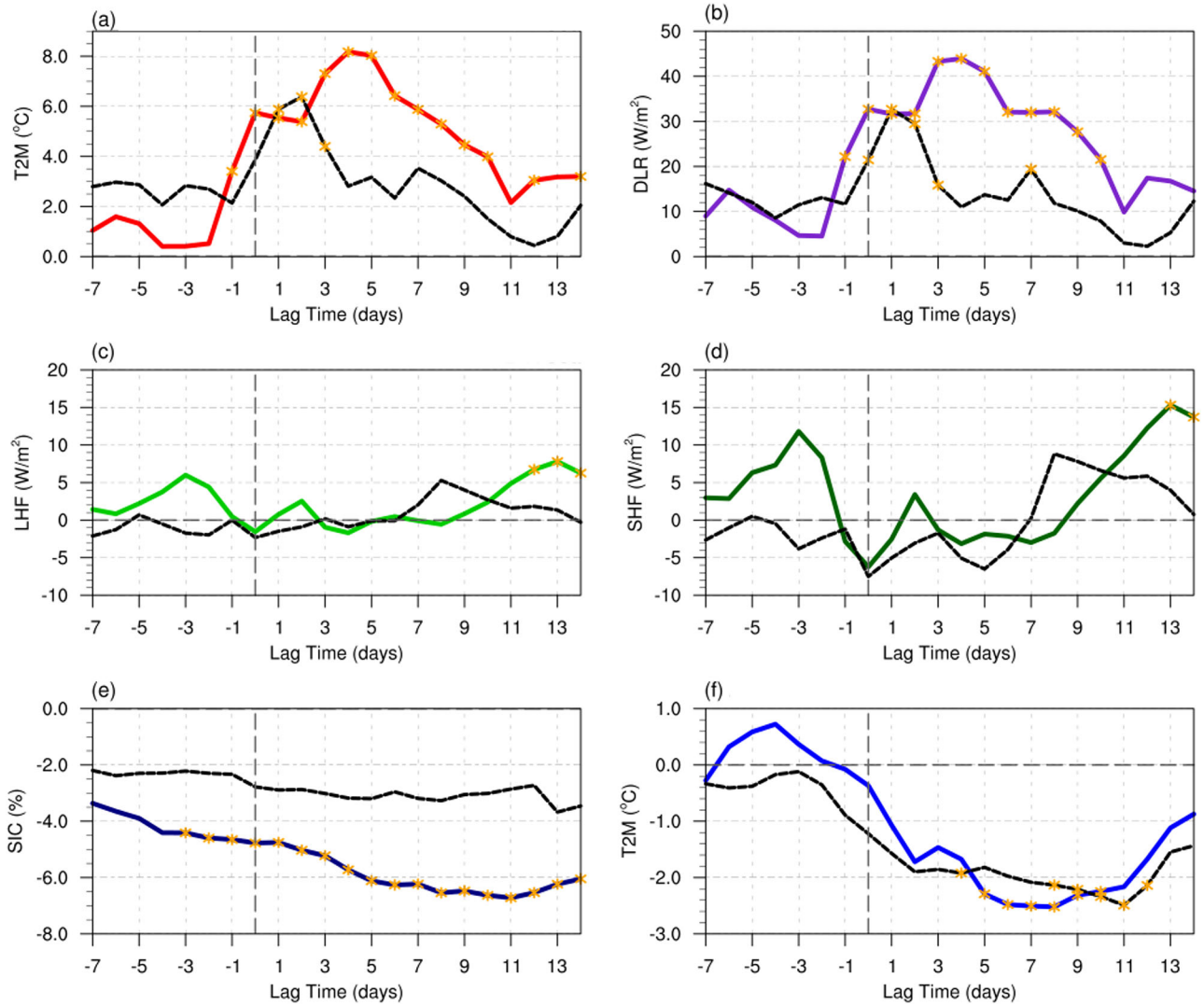

Fig. 6 | Time series of atmospheric and surface variables relative to Ural Blocking onset under SPAO and WPAO. All variables are shown from Lag −7 to Lag +14 days relative to UB onset, with SPAO composites in colored lines and WPAO composites in black lines. **a**–**e** Variables averaged over the Barents–Kara Sea (BKS; 75°–85°N, 30°–80°E): **a** 2-m temperature (T2M, °C), **b** downward longwave radiation (DLR, W/m^2), **c** latent heat flux (LHF, W/m^2), **d** sensible heat flux (SHF, W/m^2), and **e** sea ice concentration (SIC, %). **f** T2M (°C) averaged over Central Eurasia (CEU; 40°–60°N, 60°–100°E). Orange markers indicate values statistically significant at the 95% confidence level based on a two-tailed Student's *t* test.

Potential vorticity dynamics and the longevity of Ural blocking

Meridional potential vorticity gradient (PVy) is critical for regulating Rossby wave breaking and atmospheric blocking persistence[26]. A weakened PVy reduces the restoring force on planetary waves, thus supporting the formation and longevity of blocking systems such as UB[26–28]. Recently, Nie et al.[29] demonstrated that sub-seasonal sea ice anomalies and thermal forcing act to maintain the WACE pattern by increasing the persistence of the Ural anticyclonic anomaly through a reduction of the background flow and PVy.

Building on this framework, we investigate how the AO magnitude specifically modulates this PV environment through synoptic-scale storm processes, providing a more detailed dynamical engine for the observed blocking longevity. While our previous findings indicate that UB events persist longer under SPAO conditions—coinciding with intensified storm activity and amplified Arctic warming—the direct link to PVy modulation remains to be clarified. To understand the underlying dynamics, we examine whether the storm-driven thermodynamic feedback and associated circulation changes under SPAO significantly weaken PVy, thereby facilitating the prolonged life cycle of UB.

Under SPAO, pronounced PVy weakening occurs around 60°–70°N in the mid-to-upper troposphere (320–300 K; ~500–300 hPa), coinciding with the primary latitudes of UB occurrence (Fig. 7a, see also Fig. 2a). This vertically coherent PVy reduction is attributed to intensified storm-driven Arctic warming and the subsequent radiative feedback. This implies that the transient storm energy is converted into a stationary dynamical structure via PV modification. The reduced meridional PV gradient consequently weakens Rossby wave restoring forces, creating favorable conditions for blocking persistence and longevity.

To quantify the link between the initial dynamical state and blocking longevity, we calculated the event-by-event Pearson correlation coefficient (r) between the PVy anomalies at the onset date (at 320 K) and the total duration of each individual UB event. Under SPAO, a statistically significant negative relationship is highlighted within the Ural region (Fig. 7c). This indicates that under the SPAO regime, a stronger PVy reduction at the onset—pre-conditioned by robust storm-driven Arctic warming—serves as a reliable precursor for a longer-lasting UB.

Conversely, under WPAO, PVy reductions are not only weaker in magnitude but also statistically insignificant across the primary blocking-occurrence latitudes (50°–70°N; Fig. 7b). Correlation analysis (Fig. 7d)

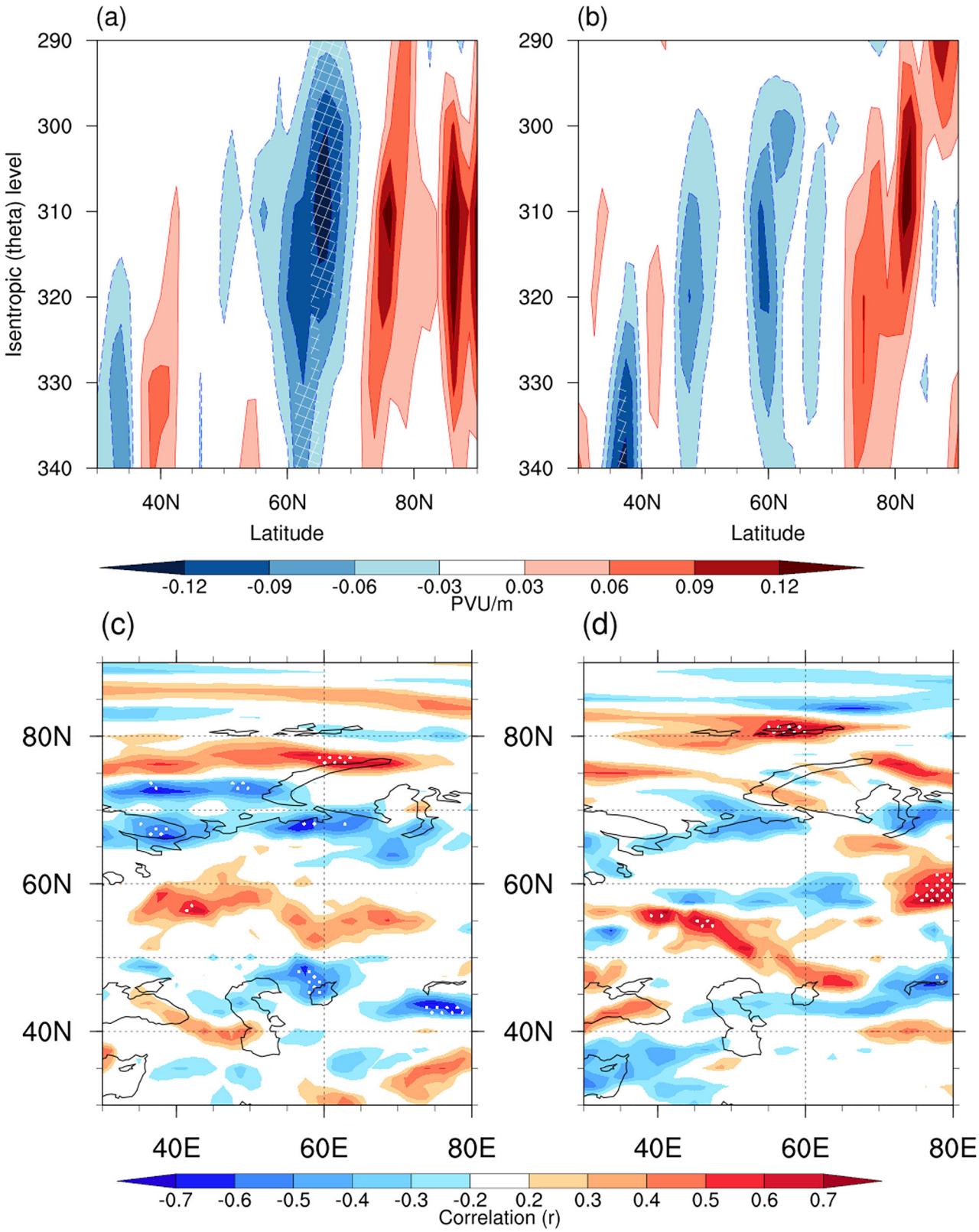

Fig. 7 | Vertical and horizontal structures of PVy anomalies and their correlation with Ural Blocking duration under different AO conditions. a, **b** Vertical–latitude cross-sections of PVy anomalies (PVU m^{-1}; 1 PVU = 10^{-6} K m^2 kg^{-1} s^{-1}) averaged over 30°–80°E on the UB onset date for **a** SPAO (18 events) and **b** WPAO (15 events). The *x*-axis indicates latitude (30°–90°N), and the *y*-axis shows isentropic levels (340–290 K). White x marks denote regions statistically significant at the 95% confidence level based on a two-tailed Student's *t* test. Horizontal distribution of the Pearson correlation coefficient (*r*) calculated between PVy anomalies at UB onset date (320 K) and the total duration (days) for **c** SPAO and **d** WPAO. White dots indicate regions where correlations are statistically significant at the 95% confidence level based on a two-tailed Student's *t* test.

similarly shows no clear connection between these initial PVy anomalies and UB duration. Following the framework of Nie et al.[29], this implies that under WPAO, the external forcing—including sea ice anomalies and thermal feedback—are insufficient to modulate the background PVy to a degree that effectively anchors the UB system.

Collectively, these findings emphasize PV dynamics' critical role in modulating UB persistence across different AO magnitudes. Specifically, significant PVy weakening and its robust negative correlation with UB duration under SPAO highlight how dynamically and thermodynamically driven PV modifications enhance blocking longevity.

Discussion

This study investigates how the magnitude of the positive AO phase modulates UB characteristics and the WACE pattern, focusing on the interplay between storm activity, Arctic warming, and PV dynamics.

A fundamental finding of this study is that the AO magnitude modulates storm trajectories, serving as the key link to the ensuing synoptic–thermodynamic chain. Our analysis reveals a distinct "steering effect": as the positive AO strengthens, the intensified jet stream acts as a coherent waveguide, channeling North Atlantic storms directly into the BKS. This highlights that the AO magnitude—not just its phase—determines the efficiency of storm-driven energy injection into the Arctic. This shift in storm organization fundamentally differentiates the maintenance mechanisms of SPAO-related and WPAO-related UB.

In SPAO UB events, the focused storm train facilitates intense poleward heat and moisture transport, triggering rapid BKS warming (peaking at +8°C) and accelerating sea ice loss. According to Kim and Kim[30], such moisture and heat advection significantly increase precipitable water and cloud cover, which are primary drivers for the enhanced DLR in the Arctic. Consistent with this mechanism, our results show a substantial enhancement of DLR (+ 40 W/m²), which creates a positive feedback loop that weakens the meridional PV gradient in the mid-to-upper troposphere.

Notably, this storm-induced feedback acts as a thermodynamic maintenance mechanism rather than an impulsive force for the initial amplification of the blocking system. According to Nonlinear Multiscale Interaction (NMI) theory, a reduced meridional PV gradient diminishes the Rossby wave restoring force, favoring the anchoring and extended persistence of the blocking system[28]. This is consistent with our finding that while SPAO significantly enhances UB longevity (6.1 days vs. 4.7 days) without necessarily increasing its peak intensity. The importance of this persistence is further supported by numerical evidence showing that realistic ice melting is essential for sustaining ocean–atmosphere interactions and extending the duration of Arctic warming[17]. Consequently, the modified PV environment under SPAO UB effectively anchors the blocking system, prolonging its life cycle at a nearly fixed location.

Conversely, WPAO UB events are associated with scattered storm tracks that offer ineffective meridional steering, failing to generate sufficient thermodynamic feedback or significant PV modification. The relatively weaker jet under WPAO facilitates the westward migration of the UB by reducing its eastward phase speed. According to Yin et al[21]., this environment suppresses synoptic eddy activities over high-latitude Eurasia, triggering a nonlinear eddy-to-mean flow feedback that maintains the Eurasian cooling. Without a stabilizing "anchor" from intense storms, this feedback-driven cooling expands and migrates westward along with the UB. This spatial displacement leads to a shorter detection period compared to the SPAO regime, even if the high-pressure system remains present.

Our findings offer crucial implications for resolving the "AO-Blocking Paradox" and improving sub-seasonal predictability. First, this study challenges the conventional view that the positive AO phase primarily suppresses high-latitude blocking due to enhanced zonal flow. We demonstrate a nonlinear, threshold-dependent mechanism: while a positive AO generally creates a zonal background, an "excessively strong" positive AO paradoxically promotes blocking persistence by efficiently injecting storm-driven energy into the Arctic. This suggests that the intensity of the jet stream is as critical as its phase in determining Arctic-midlatitude linkages.

Second, the identification of the "Storm-PV coupling" mechanism provides a new perspective on the debate regarding the drivers of the WACE pattern—whether it arises from internal atmospheric variability or boundary forcing (sea ice loss). Our results indicate that these two factors are not mutually exclusive but synergistic: strong internal variability (SPAO-driven storms) acts as the trigger, while the boundary state (sea ice loss and radiative feedback) serves as the amplifier. This implies that as the Arctic continues to warm, the efficiency of this storm-driven blocking mechanism may increase, potentially making Eurasian cold extremes more sensitive to North Atlantic storm activity even under a positive AO regime.

Finally, these results have practical applications for sub-seasonal to seasonal (S2S) forecasting. The distinct threshold behavior observed between Weak and Strong Positive AO suggests that monitoring the magnitude of the AO index, in conjunction with North Atlantic storm track coherence, could serve as an early warning signal for prolonged Eurasian cold spells. Future climate projections often anticipate a poleward shift and intensification of the eddy-driven jet; our findings suggest that such a shift might not simply reduce blocking frequency but could instead alter the nature of blocking—favoring more thermodynamically driven, persistent events initiated by intense storm intrusions. Future research should focus on how this threshold-dependent storm-blocking interaction is represented in climate models, which is essential for reducing uncertainties in projecting winter extremes under Arctic amplification.

Methods

Data

Daily reanalysis data were obtained from the Japanese 55-year Reanalysis (JRA-55[31]) for winter (December–February) during 1981/82–2022/23 (specifically, from December 1981 to February 2023). The winter season (DJF) includes December of the previous year and January and February of the current year. The dataset includes the following variables: 2-m temperature (T2M), sea level pressure (SLP), 500-hPa geopotential height (GPH), 850-hPa temperature (T850), 850-hPa relative vorticity, zonal and meridional wind components (U, V), downward longwave radiation (DLR), latent heat flux (LHF), sensible heat flux (SHF), and potential vorticity (PV). All variables were analyzed at a horizontal resolution of 1.25° × 1.25°.

Daily Sea Ice Concentration (SIC) data were retrieved from the NOAA Optimum Interpolation (OI) Sea Surface Temperature (SST) V2 High-Resolution Dataset[32] for the same period. The SIC data, originally at 0.25° × 0.25° resolution, were remapped to 1.0° × 1.0° resolution to balance computational efficiency and spatial representation. Further details are available at the NOAA Physical Sciences Laboratory (PSL).

Daily Arctic Oscillation (AO), North Atlantic Oscillation (NAO) indices were obtained from the Climate Prediction Center (CPC) for the winters of 1982–2023.

Region definition

For quantitative analysis, specific regions were defined as follows: the Barents-Kara Sea (BKS; 75°–85°N, 30°–80°E) for Arctic temperature and sea ice concentration changes, and Central Eurasia (CEU; 40°–60°N, 60°–100°E) for mid-latitude temperature responses.

Ural blocking detection

To detect Ural blocking (UB) events during winter, we used the Regional Hybrid (RHYB) blocking detection method. The RHYB method is a modification of the original Hybrid detection (HYB) method[33] to account for regional variability in atmospheric circulation. In the original HYB algorithm, the amplitude threshold is derived from the domain-averaged standard deviation of 500-hPa geopotential height anomalies over the Northern Hemisphere (30°–90° N); for the winter months (DJF), this uniform threshold typically ranges between 220 and 230 gpm.

However, monthly standard deviation (σ) fields of geopotential height anomalies show significant regional differences across the Northern

Hemisphere, with the North Atlantic and North Pacific exhibiting much higher variability (over 110 and 130 gpm, respectively) compared to Eurasia (50–100 gpm) (Figure. S6). Despite these regional differences, the original HYB method applies a uniform threshold across the Northern Hemisphere, potentially causing under-detection of blocking events in low-variability regions (e.g., Eurasia) and over-detection in high-variability regions (e.g., the North Atlantic).

To address the limitations of a uniform threshold, the RHYB method applies a region-specific threshold defined as 2.0σ at each grid point. However, in low-variability regions, such as the midlatitudes of East Asia, applying only the 2.0σ criterion may result in the false detection of weak, transient ridges. To prevent over-detection of dynamically insignificant system, an absolute minimum threshold of 170 gpm is enforced; thus, the effective threshold at each grid point is determined as the larger value between the local 2.0σ and 170 gpm.

RHYB retains the main features of the HYB algorithm, including the identification of flow reversal and tracking criteria, while modifying only the thresholds to account for regional variability. A blocking event is initially identified based on three criteria: a total lifecycle of at least five consecutive days, a minimum spatial scale of 2.5×10^6 km², and an area overlap of at least 50% between consecutive days[34]. Among these identified events, we specifically define Ural blocking as those events where the blocking center remains within the Ural region (30°–80°E, 30°–90°N) for at least three days during its lifecycle. By applying the RHYB method, a total of 67 UB events were identified for the 42 winters (December–February) during 1981/82–2022/23. A more detailed description and technical validation of the RHYB method will be presented in a separate manuscript currently under review.

Arctic oscillation classification

To determine the background AO conditions associated with each UB events, we averaged the CPC daily AO index over a 5-day window from 7 to 3 days prior to the UB onset, following the lag relationship identified by Luo et al. (2016a). Specifically, UB events were categorized based on this 5-day mean AO magnitude: events exceeding +1.0 (approximately 0.55 σ_{5d} of the wintertime mean) were classified as Strong Positive AO (SPAO) UB (18 events), while those between 0 and +1.0 were classified as Weak Positive AO (WPAO) UB (15 events).

North Atlantic storm tracking

To examine the impact of Atlantic storms on UB, we identified Atlantic storms using JRA-55 reanalysis data for winter seasons from 1981/82 to 2022/23. The study employed 850-hPa relative vorticity and mean sea level pressure fields at a 1.25° × 1.25° spatial resolution for storm detection. The detection and tracking method, adapted from Hong et al.[15] and modified from Vitart et al.[35], is optimized for identifying extratropical storms in the Northern Hemisphere.

The storm detection procedure involved: (1) identifying candidate storm centers every 6 h using local maxima of 850-hPa relative vorticity ($<2.0 \times 10^{-5}$ s^{-1}) and the nearest local minima of mean sea level pressure within a 400-km radius; (2) tracking storms by locating subsequent centers within a 750-km radius of the previous position; and (3) reconstructing storm life cycles by connecting tracked centers to form complete trajectories. Storms were filtered for the cyclogenesis region (25°–65°N, 30°W–30°E) with minimum lifetimes of ≥48 h and travel distances of ≥1000 km.

Data availability

The Japanese 55-year Reanalysis (JRA-55) daily data used in this study were obtained from the University Corporation for Atmospheric Research (UCAR) Geoscience Data Exchange (GDEX) at https://gdex.ucar.edu/datasets/d628000/. The NOAA Optimum Interpolation (OI) Sea Surface Temperature (SST) V2 High-Resolution dataset was provided by the National Centers for Environmental Information (NOAA/NCEI) and is accessible at https://www.ncei.noaa.gov/data/sea-surface-temperature-optimum-interpolation/v2.1/access/avhrr/. The Arctic Oscillation (AO) and North Atlantic Oscillation (NAO) indices were obtained from the NOAA Climate Prediction Center (CPC) at https://www.cpc.ncep.noaa.gov/products/precip/CWlink/daily_ao_index/teleconnections.shtml.

Received: 4 December 2025; Accepted: 7 March 2026;
Published online: 24 March 2026

References

1. Thompson, D. W. & Wallace, J. M. The Arctic Oscillation signature in the wintertime geopotential height and temperature fields. *Geophys. Res. Lett.* **25**, 1297–1300 (1998).
2. Thompson, D. W. & Wallace, J. M. Regional climate impacts of the Northern Hemisphere annular mode. *Science* **293**, 85–89 (2001).
3. Ahmadi, R. & Alizadeh, O. The possible links between the Barents–Kara sea-ice area, Ural blocking, and the North Atlantic Oscillation. *Q. J. R. Meteorol. Soc.* **149**, 3357–3372 (2023).
4. Zhou, X., Sato, T. & Li, S. Interannual variation of the Warm Arctic–Cold Eurasia pattern modulated by Ural blocking and the North Atlantic Oscillation under changing sea ice conditions. *Prog. Earth Planet. Sci.* **10**, 59 (2023).
5. Luo, D. et al. Impact of Ural blocking on winter warm Arctic–cold Eurasian anomalies. Part II: the link to the North Atlantic Oscillation. *J. Clim.* **29**, 3949–3971 (2016a).
6. He, S. et al. Impact of Arctic Oscillation on the East Asian climate: a review. *Earth-Sci. Rev.* **164**, 48–62 (2017).
7. Gong, T. & Luo, D. Ural blocking as an amplifier of the Arctic sea ice decline in winter. *J. Clim.* **30**, 2639–2654 (2017).
8. Cheung, H. N., Zhou, W., Mok, H. Y. & Wu, M. C. Relationship between Ural–Siberian blocking and the East Asian winter monsoon in relation to the Arctic Oscillation and the El Niño–Southern Oscillation. *J. Clim.* **25**, 4242–4257 (2012).
9. Hassanzadeh, P. & Kuang, Z. Blocking variability: Arctic amplification versus Arctic oscillation. *Geophys. Res. Lett.* **42**, 8586–8595 (2015).
10. Cheung, H. H. et al. A strong phase reversal of the Arctic Oscillation in midwinter 2015/2016: Role of the stratospheric polar vortex and tropospheric blocking. *J. Geophys. Res. Atmos.* **121**, 13443–13460 (2016).
11. Li, C., Zhang, Q., Ji, L. & Peng, J. Interannual variations of the blocking high over the Ural Mountains and its association with the AO/NAO in boreal winter. *Acta Meteorol. Sin.* **26**, 163–175 (2012).
12. You, C., Tjernström, M., Devasthale, A. & Steinfeld, D. The role of atmospheric blocking in regulating Arctic warming. *Geophys. Res. Lett.* **49**, e2022GL097899 (2022).
13. Zhang, X. et al. Arctic cyclones have become more intense and longer-lived over the past seven decades. *Commun. Earth Environ.* **4**, 348 (2023).
14. Kim, B. M. et al. Major cause of unprecedented Arctic warming in January 2016: critical role of an Atlantic windstorm. *Sci. Rep.* **7**, 40051 (2017).
15. Hong, J. Y. et al. A critical role of extreme Atlantic windstorms in Arctic warming. *Asia-Pac. J. Atmos. Sci.* **56**, 17–28 (2020).
16. Overland, J. E. et al. How do intermittency and simultaneous processes obfuscate the Arctic influence on midlatitude winter extreme weather events? *Environ. Res. Lett.* **16**, 045010 (2021).
17. Park, J. H. et al. Impact of Arctic sea ice representation on extended medium-range forecasting: a case study of the 2016 Barents-Kara Sea warming event. *Asia-Pac. J. Atmos. Sci.* **61**, 5 (2025).
18. Luo, B., Luo, D., Wu, L., Zhong, L. & Simmonds, I. Atmospheric circulation patterns which promote winter Arctic sea ice decline. *Environ. Res. Lett.* **12**, 054017 (2017).
19. Kautz, L. A. et al. Atmospheric blocking and weather extremes over the Euro-Atlantic sector–A review. *Weather Clim. Dynam.* **2**, 305–336 (2021).
20. Murto, S., Caballero, R., Svensson, G. & Papritz, L. Interaction between Atlantic cyclones and Eurasian atmospheric blocking drives

wintertime warm extremes in the high Arctic. *Weather Clim. Dynam.* **3**, 21–44 (2022).
21. Yin, M. et al. Amplified wintertime Arctic warming causes Eurasian cooling via nonlinear feedback of suppressed synoptic eddy activities. *Sci. Adv.* **11**, eadr6336 (2025).
22. Hall, R., Erdélyi, R., Hanna, E., Jones, J. M. & Scaife, A. A. Drivers of North Atlantic Polar Front jet stream variability. *Int. J. Climatol.* **35**, 1697–1720 (2015).
23. Stendel, M., Francis, J., White, R., Williams, P. D. & Woollings, T. in *Climate Change* (eds. Letcher, T. M.) 327–357 (Elsevier, 2021).
24. Luo, D. et al. Impact of Ural blocking on winter warm Arctic–cold Eurasian anomalies. Part I: blocking-induced amplification. *J. Clim.* **29**, 3925–3947 (2016b).
25. Tyrlis, E. et al. On the role of Ural Blocking in driving the Warm Arctic–Cold Siberia pattern. *Q. J. R. Meteorol. Soc.* **146**, 2138–2153 (2020).
26. Luo, D. et al. Weakened potential vorticity barrier linked to recent winter Arctic sea ice loss and midlatitude cold extremes. *J. Clim.* **32**, 4235–4261 (2019).
27. Luo, D., Chen, X., Dai, A. & Simmonds, I. Changes in atmospheric blocking circulations linked with winter Arctic warming: A new perspective. *J. Clim.* **31**, 7661–7678 (2018).
28. Luo, D. & Zhang, W. A nonlinear multiscale theory of atmospheric blocking: dynamical and thermodynamic effects of meridional potential vorticity gradient. *J. Atmos. Sci.* **77**, 2471–2500 (2020).
29. Nie, Y., Ren, H., Zhang, Y. & Zhang, P. Roles of atmospheric variability and arctic sea ice in the asymmetric Arctic–Eurasia temperature connection on subseasonal time scale. *J. Clim.* **35**, 7575–7594 (2022).
30. Kim, H. M. & Kim, B. M. Relative contributions of atmospheric energy transport and sea ice loss to the recent warm Arctic winter. *J. Clim.* **30**, 7441–7450 (2017).
31. Kobayashi, S. et al. The JRA-55 reanalysis: general specifications and basic characteristics. *J. Meteorol. Soc. Jpn. Ser. II* **93**, 5–48 (2015).
32. Huang, B. et al. Improvements of the daily optimum interpolation sea surface temperature (DOISST) version 2.1. *J. Clim.* **34**, 2923–2939 (2021).
33. Dunn-Sigouin, E., Son, S. W. & Lin, H. Evaluation of Northern Hemisphere blocking climatology in the global environment multiscale model. *Mon. Weather Rev.* **141**, 707–727 (2013).
34. Kim, S. H. et al. Contribution of Ural and Kamchatka blockings to the amplified warm Arctic–Cold Eurasia pattern under Arctic Sea ice loss and Eurasian cooling. *J. Clim.* **35**, 4071–4083 (2022).
35. Vitart, F., Anderson, J. L. & Stern, W. F. Simulation of interannual variability of tropical storm frequency in an ensemble of GCM integrations. *J. Clim.* **10**, 745–760 (1997).

Acknowledgements

This work was funded by the Republic of Korea-NOAA Joint Project Agreement (JPA) Polar Panel, Task Number P91 “Comparative understanding of Arctic-Midlatitude Weather Connections occurring over United States and Korea in recent decades”. This work was funded by the Korea Meteorological Administration Research and Development Program under Grant RS-2025-02313090. M. Wang is funded with support of the Arctic Research Program of the NOAA Global Ocean Monitoring and Observing (GOMO) office through the Cooperative Institute for Climate, Ocean, & Ecosystem Studies (CICOES) under NOAA Cooperative Agreement NA20OAR4320271, Contribution No 2025-1449, and Pacific Marine Environmental Laboratory (PMEL) Contribution No. 5768. S.J. Kim was supported by PE26010 of Korea Polar Research Institute.

Author contributions

B.M.K. conceived the study, provided supervision, developed the Regional Hybrid (RHYB) blocking detection method, and served as the corresponding author. H.Y.K. performed the primary data analysis and visualization and wrote the initial draft of the manuscript. H.N. assisted with the methodology, including the development of the RHYB method, and reviewed the manuscript. M.W., J.O., and S.J.K. provided critical expertise and advice on Arctic climate dynamics and extreme events, contributed to the interpretation of the results, and reviewed and revised the manuscript. All authors approved the final submission.

Competing interests

The authors declare no competing interests.

Additional information

Supplementary information The online version contains supplementary material available at https://doi.org/10.1038/s41612-026-01384-x.

Correspondence and requests for materials should be addressed to Baek-Min Kim.